






Phase transitions study of the liquid crystal DIO with a ferroelectric nematic, a nematic, and an intermediate phase and of mixtures with the ferroelectric nematic compound RM734 by adiabatic scanning calorimetry

J. Thoen ^{1,*}, G. Cordoyiannis ², W. Jiang ³, G. H. Mehl ³ and C. Glorieux ¹

¹Laboratory for Soft Matter and Biophysics, Department of Physics and Astronomy, KU Leuven, Celestijnenlaan 200D, 3001 Leuven, Belgium

²Condensed Matter Physics Department, Jožef Stefan Institute, 1000 Ljubljana, Slovenia

³Department of Chemistry, University of Hull, Hull HU6 7RX, United Kingdom



(Received 18 October 2022; accepted 21 December 2022; published 12 January 2023)

High-resolution calorimetry has played a significant role in providing detailed information on phase transitions in liquid crystals. In particular, adiabatic scanning calorimetry (ASC), capable of providing simultaneous information on the temperature dependence of the specific enthalpy $h(T)$ and on the specific heat capacity $c_p(T)$, has proven to be an important tool to determine the order of transitions and render high-resolution information on pretransitional thermal behavior. Here we report on ASC results on the compound 2,3',4',5'-tetrafluoro[1,1'-biphenyl]-4-yl 2,6-difluoro-4-(5-propyl-1,3-dioxan-2-yl) benzoate (DIO) and on mixtures with 4-[(4-nitrophenoxy)carbonyl]phenyl 2,4-dimethoxybenzoate (RM734). Both compounds exhibit a low-temperature ferroelectric nematic phase (N_F) and a high-temperature paraelectric nematic phase (N). However, in DIO these two phases are separated by an intermediate phase (N_x). From the detailed data of $h(T)$ and $c_p(T)$, we found that the intermediate phase was present in all the mixtures over the complete composition range, albeit with strongly decreasing temperature width for that phase with decreasing mole fraction of DIO (x_{DIO}). The x_{DIO} dependence on the transition temperatures for both transitions could be well described by a quadratic function. Both these transitions were weakly first order. The true latent heat of the $N_x - N$ transition of DIO was as low as $L = 0.0075 \pm 0.0005$ J/g and $L = 0.23 \pm 0.03$ J/g for the $N_F - N_x$ transition, which is about twice the previously reported value of 0.115 J/g for the $N_F - N$ transition in RM734. In the mixtures both transition latent heats decrease gradually with decreasing x_{DIO} . At all the $N_x - N$ transitions pretransition fluctuation effects are absent and these transitions are purely but very weakly first order. As in RM734 the transition from the N_F to the higher-temperature phase exhibits substantial pretransitional behavior, in particular, in the high-temperature phase. Power-law analysis of $c_p(T)$ resulted in an effective critical exponent $\alpha = 0.88 \pm 0.1$ for DIO and this value decreased in the mixtures with decreasing x_{DIO} toward $\alpha = 0.50 \pm 0.05$ reported for RM734. Ideal mixture analysis of the phase diagram was consistent with ideal mixture behavior provided the total transition enthalpy change was used in the analysis.

DOI: [10.1103/PhysRevE.107.014701](https://doi.org/10.1103/PhysRevE.107.014701)

I. INTRODUCTION

Thermotropic liquid crystals are materials characterized by different degrees of orientational and partial positional order between crystalline solids and the isotropic liquid state [1]. The simplest liquid crystal phase is the nematic phase, as the least ordered phase, where rodlike or disklike molecules are statistically oriented along a common direction, called the director, whereas the centers of mass of the molecules are randomly distributed. Depending on the shape of the molecules or molecular aggregates, on the absence or presence of dipoles, on temperature, and on mixture composition, different types of nematic phases are encountered. For example, phase transitions between uniaxial and biaxial nematic phases [2,3] as well as between two uniaxial nematic phases with different types of short-range smectic order [4] have been observed. Although Debye [5] and Born [6] already

discussed more than a century ago the possibility of orientational order of polar rod-shaped molecules of a nematic phase with interacting molecular dipoles in such a way that the nematic phase is ferroelectric with a nonzero polarization density, such a phase has never been observed until recently. In 2017 two independent reports by Mandle *et al.* [7] and Nishikawa *et al.* [8] claimed the discovery of a new type of nematic phase for two quite different types of molecules. The two compounds that were subsequently extensively studied [8–18] are RM734 (4-[(4-nitrophenoxy)carbonyl]phenyl 2,4-dimethoxybenzoate) [7] and DIO (2,3',4',5'-tetrafluoro[1,1'-biphenyl]-4-yl 2,6-difluoro-4-(5-propyl-1,3-dioxan-2-yl) benzoate) [8]. The chemical structures of DIO and RM734 are given in Fig. 1. The strongly polar compound RM734 exhibits two nematic phases separated by a phase transition, which was claimed to be weakly first order [13]. In 2020 Chen *et al.* [14] presented experimental evidence for ferroelectricity in the low-temperature nematic phase (N_F) of RM734, the high-temperature one being a normal uniaxial nematic phase (N). The compound DIO is special in the sense that in ad-

*jan.thoen@kuleuven.be

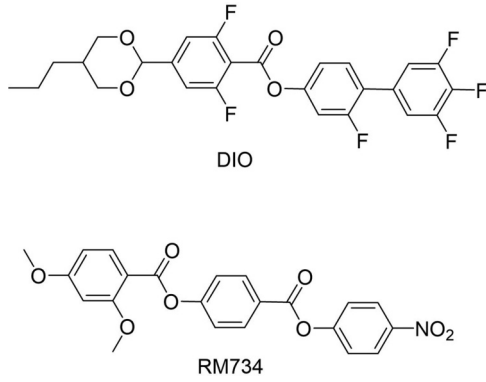


FIG. 1. Chemical structure of DIO (top) and RM734 (bottom).

dition to the “ferroelectriclike” [8] N_F phase, it exhibits at low temperatures an additional phase between the N_F phase and the normal nematic phase N . During the past two years the quest for new liquid crystals with ferroelectric nematic phases and their investigations gained substantial momentum. Efforts have largely concentrated on synthesizing variants of the RM734 and DIO families, to the extent that presently more than 50 molecules are known to induce ferroelectricity [19–22]. These quests for new materials are accompanied by extensive studies of new polarization related phenomena and applications [23–28].

The true nature and proper naming of the intermediate phase is presently a matter of debate. In [8] it was initially called M_2 and subsequently N_x in [17]. In a paper by Chen *et al.* [29] it was claimed, on the basis of structural characterization, that the intermediate phase of DIO (M_2 in [8] and N_x in [17]), between the high-temperature (polar-disordered) dielectric nematic phase and the low-temperature (polar-ordered) ferroelectric nematic phase N_F , is an antiferroelectric smectic phase with the nematic director and the polarization oriented parallel to smectic layer planes, and the polarization alternating in sign from layer to layer. This phase was termed smectic Z_A and indicated as $\text{Sm}Z_A$. However, in a very recent paper Sebastián *et al.* [30] argued that the intermediate phase of DIO should be considered as a splay nematic phase and be named N_S . Because calorimetry cannot render information on the structure of phases, and in view of the above variation in naming of the intermediate phase, we will, further in this paper, use the terminology N_x to indicate this intermediate phase between the N and N_F phases. In another recent paper, Chen *et al.* [31] reported on experimental investigations of the phase diagram and electro-optics of binary mixtures of RM734 and DIO, and found complete miscibility in the dielectric nematic as well as in the ferroelectric nematic phases.

In recent high-resolution adiabatic scanning calorimetric measurements of the N_F - N transition of RM734, reported by Thoen *et al.* [32], the order of the transition as well as the pretransitional fluctuation-induced critical behavior was investigated in detail. The N_F - N transition was found to be very weakly first order with a latent heat $L = 0.115 \pm 0.005$ J/g (which is more than an order of magnitude smaller than the values derived from differential scanning calorimetry (DSC) [13,14]). In both the N and N_F phases the power-law

analysis of the specific heat capacity c_p resulted in an effective critical exponent $\alpha = 0.50 \pm 0.05$ and an amplitude ratio $A_{N_F}/A_N = 0.42 \pm 0.03$. The very small latent heat and the value of α indicate the N_F - N transition in RM734 to be close to a tricritical point. This conclusion was additionally supported by an order parameter critical exponent value of $\beta \approx 0.25$ obtained from electric polarization measurements in the N_F phase (Ref. [32] in [32]).

DSC measurements have indicated the N_F - N_x and the N_x - N transitions of DIO to be first order. However, it should be realized that it is inherently difficult for DSC to distinguish between true latent heats and pretransitional fluctuation-induced enthalpy increases [33,35]. In view of that, we present here results for DIO and for its mixtures with RM734 of simultaneous measurements of the temperature dependence of the specific heat capacity $c_p(T)$ and of the specific enthalpy $h(T)$ by high-resolution adiabatic scanning calorimetry (ASC). The high-resolution data of $c_p(T)$ and $h(T)$ near both phase transitions, N_F - N_x and N_x - N , will be used to determine the order of the transitions and characterize the pretransitional critical behavior.

II. EXPERIMENT

A. Adiabatic scanning calorimetry (ASC)

1. Operational principle

ASC is used to obtain simultaneously and continuously the temperature evolution of the heat capacity C_p and the enthalpy H of a sample under investigation [33–37]. The basic concept of ASC is in applying a constant heating or cooling power to a sample holder containing the sample. The sample holder is placed inside a surrounding adiabatic shield; in practice this is implemented by a number of shields and by continuously vacuum pumping the calorimeter. In a heating run, the heat exchange between inner shield and sample holder is canceled by keeping the temperature difference zero at all times. In a cooling run the heat exchange is controlled and monitored. During a run, the sample temperature $T(t)$ is recorded as a function of time t . Together with the applied power P this directly results in the enthalpy curve

$$H(T) - H(T_0) = \int_{t_0}^{t(T)} P dt = P[t(T) - t_0(T_0)], \quad (1)$$

where $H(T_0)$ is the enthalpy of the system at temperature T_0 at the starting time t_0 of the run. The heat capacity $C_p(T)$ is easily calculated via the ratio of the known constant power P and the changing temperature rate $\dot{T} = dT/dt$,

$$C_p = \frac{P}{\dot{T}}. \quad (2)$$

The specific heat capacity $c_p(T)$ and the specific enthalpy $h(T)$ are obtained by using the sample mass and the calibrated background values of the empty calorimeter and of the used sample cells. It should be noted that keeping P constant in Eq. (2) is completely opposite to the operation of a DSC where one imposes a constant scanning rate \dot{T} on a sample and on a reference and measures the difference in heat flux, $\Delta P(t)$, between the sample and the reference.

2. Peltier-element-based adiabatic scanning calorimeter (pASC)

Maintaining adiabatic conditions over a long time and over wide temperature ranges as implemented in “classical” versions of ASC is challenging. Detailed descriptions of this type of implementation and experimental results can be found in [33–37] and references therein. However, in the last decade this approach has been superseded by the development of the Peltier-element-based adiabatic scanning calorimeter (pASC), providing greater user friendliness and allowing much wider temperature ranges as well as much smaller samples [38–42].

In a pASC the uncertainty on the final results, $c_p(T)$ and $h(T)$, depends on the uncertainties on the measured quantities $T(t)$, $P(t)$, the sample mass m , and the heat capacity of the addenda C_{add} . It is assumed that the error on the time t is negligible. The addenda of the calorimeter are the sample cell and the sample holder, consisting of a thin copper supporting platform with the heater, the thermistor, and the top plate of the Peltier element. In order to assure good thermal contact between the bottom of the sample cell and the platform, a small amount (typically of the order of 1 mg) of thermal paste is applied. In extended separate runs of the calorimeter the heat capacity of the sample holder, as well as the specific heat capacity of the sample cell material and of the thermal paste, have been evaluated. From an extended error analysis presented in Ref. [43] and its supplemental material it was concluded that a relative standard uncertainty of 2% could be assigned to c_p and h , provided the uncertainty on the sample mass is kept below this value.

B. Measurements and sample preparation

Measurements have been carried out with the same pASC as the one used for the measurements on neat RM734 [32]. Samples (used as received) were transferred into stainless steel sample holders (Mettler Toledo 120 μl medium pressure crucibles) and hermetically sealed. These crucibles were vacuum tight closed with a miniature elastic O-ring between the cell body and a lid. Mixtures were prepared in the sample holders. The different masses were measured using a Mettler Toledo balance with a precision of 0.1 mg. The amounts of samples (typically 50 mg) used were chosen such that the total uncertainty was within 1%. In order to ensure proper mixing, the closed filled crucibles were placed on top of a hot plate at a temperature above the nematic-isotropic transition temperature. Subsequently, the crucible with the sample was positioned upside down on the hot plate for some time, and reversed to its normal position. This procedure was typically repeated ten times, and took between 15 and 30 min.

III. RESULTS

A. Neat DIO

1. Melting transition

After a sample cell with a pure DIO sample was mounted in the calorimeter, the calorimeter was heated to 115 $^{\circ}\text{C}$. This resulted in melting of the sample from the solid phase into the nematic phase via a sharp first-order transition at 95.8 $^{\circ}\text{C}$. In Fig. 2 the temperature dependence of the specific enthalpy and of the corresponding effective specific heat capacity are

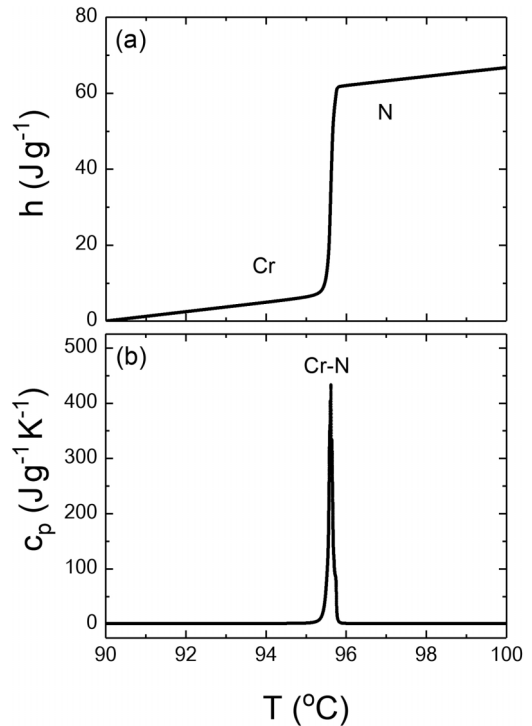


FIG. 2. Adiabatic scanning calorimetry results above and below the melting transition temperature of neat DIO, upon heating at an average rate of 0.056 K/min. Temperature dependence of the specific enthalpy $h(T)$ in panel (a) and of effective specific heat capacity $c_p(T)$ in panel (b) of neat DIO across the first-order transition from the solid crystalline phase to the nematic phase.

displayed. A detailed analysis of the data resulted in a latent heat of 54.9 ± 0.3 J/g. The cusp in the enthalpy curve at the high-temperature side of the transition is much sharper than on the low-temperature side where some curvature is observed. This is a general aspect seen at many melting transitions [39] and which is, in particular, noticed in the melting of alkane compounds [42].

A slow cooling run (at an average rate of -0.04 K/min) was subsequently started at 115 $^{\circ}\text{C}$. This resulted in clear observations of the transitions from the N to the N_x and from the N_x to the N_F phases. However, the sample solidified at a temperature of 59 $^{\circ}\text{C}$. Remelting (by heating to a temperature above 100 $^{\circ}\text{C}$) and subsequently cooling always resulted (at our slow scanning rates) in solidification between 55 $^{\circ}\text{C}$ and 60 $^{\circ}\text{C}$. Cooling to a temperature of 60 $^{\circ}\text{C}$ allowed us to carry out slow heating runs from well into the N_F phase to well into the paraelectric N phase. Several heating and cooling runs [at different values of the power P in Eqs. (1) and (2) resulting in different average rates] were executed on different samples while the samples were in the subcooled monotropic phase. Good consistency regarding $h(T)$ and $c_p(T)$ was observed between the results for different runs and samples. However, some mild and progressive downward shift of the transition temperatures was observed, in particular, when the samples were kept for prolonged times (of the order of several days) at high T in the N phase. The observed shifts were typically of a few tenths of a degree over the timescale of a week and not relevant for a specific heating or cooling run.

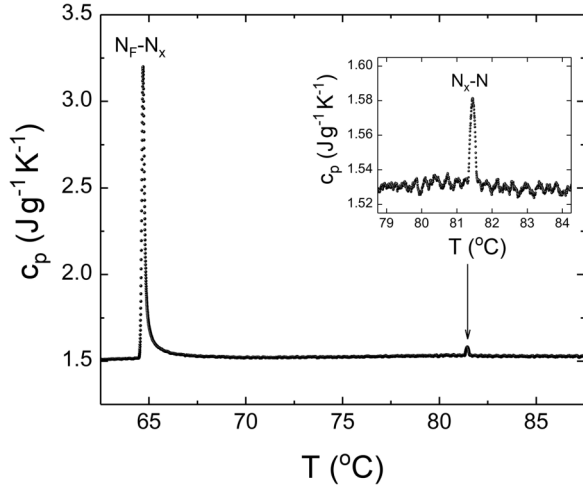


FIG. 3. Adiabatic scanning calorimetry results for neat DIO at an average heating rate of 0.058 K/min. Overview of the temperature dependence of the effective specific heat capacity $c_p(T)$ between 60 °C and 90 °C crossing the $N_F - N_x$ and the $N_x - N$ transitions. The inset gives the detailed behavior around the $N_x - N$ transition.

2. Ferroelectric nematic N_F to the intermediate N_x transition

Figure 3 gives an overview of the temperature dependence of the specific heat capacity $c_p(T)$ over the temperature range between 60 °C and 90 °C, covering both the transition from the ferroelectric N_F to the intermediate N_x phase and from the N_x to the nematic phase. In this overview figure the peak of the $N_x - N$ transition is extremely small in comparison with the $N_F - N_x$ transition (but more visible in the inset). Figure 4 gives an overview of the transition-related specific enthalpy $h(T)$ variation over the $N_F - N_x$ transition. Detailed analysis of $h(T)$ in combination with $c_p(T)$ revealed a small 0.12 ± 0.03 K two-phase region and a true latent heat of 0.23 ± 0.03 J/g, indicating the weakly first-order character of this transition. Above this transition (in the N_x phase),

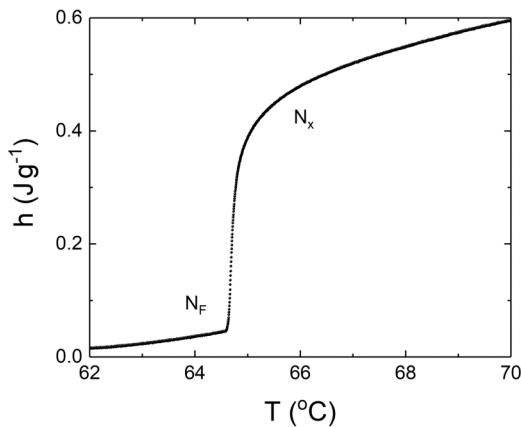


FIG. 4. Adiabatic scanning calorimetry results for neat DIO at an average heating rate of 0.058 K/min. Temperature dependence of the specific enthalpy $h(T)$ across the transition from the ferroelectric nematic N_F phase to the N_x phase after subtraction (for display reasons) of a linear temperature background $1.5(T - T_{ref})$ (J/g), with T_{ref} an arbitrary reference temperature.

substantial fluctuation-induced enthalpy variation is observed. Such variation is substantially weaker in the N_F phase. This indicates that the total, transition-related enthalpy change is composed of two contributions: the true latent heat L and the pretransitional part δh . The total enthalpy change Δh_{tr} over the transition (typically obtained in DSC) is the sum of both; thus

$$\Delta h_{tr} = L + \delta h. \tag{3}$$

In order to obtain the transition enthalpy change Δh_{tr} , it is necessary to separate it from the enthalpy change that would occur without the transition. Indeed, when one has a constant background specific heat capacity c_b , the enthalpy increases linearly with temperature. In general, c_b can depend on temperature and usually a linear dependence is chosen (much like a baseline choice in DSC) between $c_p(T_1)$ and $c_p(T_2)$ well below and well above the transition, leading to

$$c_b(T) = c_p(T_1) + \frac{c_p(T_2) - c_p(T_1)}{T_2 - T_1}(T - T_1). \tag{4}$$

In this equation, a linear temperature dependence is assumed, but not required. In some cases different choices are more appropriate, in particular, when there are substantial differences in specific heat capacity background values between the low- and high-temperature phases [42]. Subtraction of $c_b(T)$ from the $c_p(T)$ peak and integration gives

$$\Delta h_{tr} = \int_{T_1}^{T_2} [c_p(T) - c_b(T)]dT. \tag{5}$$

Alternatively, one can use the direct specific enthalpy $h(T)$ data via

$$\Delta h_{tr} = h(T_2) - h(T_1) - \int_{T_1}^{T_2} c_b(T)dT. \tag{6}$$

Using both approaches we obtained for Δh_{tr} a value of 0.48 ± 0.03 J/g. In turn this resulted in $\delta h = 0.25 \pm 0.03$ J/g by subtracting the latent heat value. Applying the same procedures to the data of RM734 [32] resulted in $\Delta h_{tr} = 1.03 \pm 0.1$ J/g and in $\delta h = 0.91 \pm 0.1$ J/g. The choices made for the values T_1 and T_2 are to some extent arbitrary and they are very important only for small peaks. We typically use values of 5 K above and below the transition temperature. The quoted uncertainties reflect reasonable variations in these temperatures.

3. Intermediate N_x to paraelectric nematic N transition

As already observed in Fig. 3, the enthalpy change associated with the transition between the N_x and the N phase must be extremely small. Nevertheless, ASC is quite capable of giving a clear picture of $h(T)$ and of $c_p(T)$ around the transition. This can be seen in the detailed Fig. 5 in the temperature range between 80.5 °C and 83 °C. A clear first-order enthalpy discontinuity with a latent heat of 0.0075 ± 0.0005 J/g and a two-phase region of 0.11 ± 0.03 K are observed. The transition is purely first order without pretransitional fluctuation contributions.

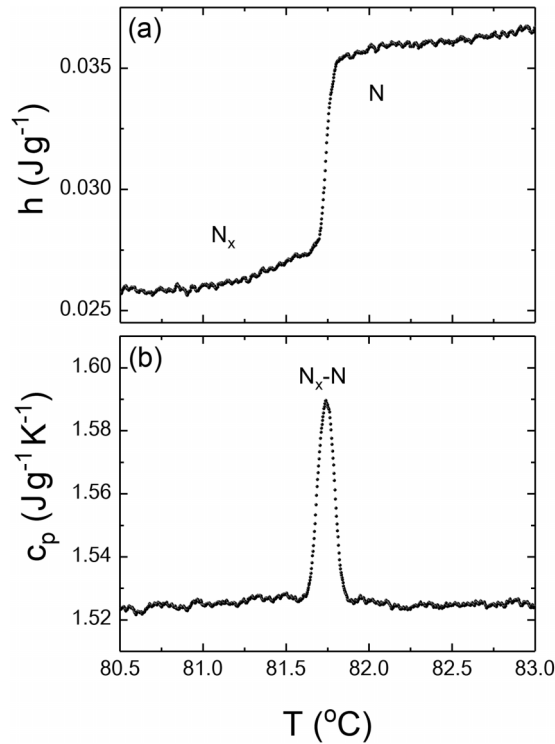


FIG. 5. Adiabatic scanning calorimetry results for neat DIO at an average heating rate of 0.058 K/min. The temperature dependence of the specific enthalpy $h(T)$ in panel (a) and the effective specific heat capacity $c_p(T)$ in panel (b) are shown across the very small first-order transition from the N_x phase to the nematic phase N . From the data of $h(T)$ a linear temperature dependent background $1.5(T - T_{\text{ref}})$ (J/g), with T_{ref} an arbitrary reference temperature, has been subtracted.

4. Anomalous pretransitional specific heat capacity behavior at the $N_F - N_x$ transition

Although the $N_F - N_x$ transition turns out to be weakly first order, from the data displayed in Figs. 3 and 4 it is obvious that substantial pretransitional fluctuations effects, in particular, in the high-temperature phase, are present. In analogy with what can be done for purely second-order phase transitions, one can try to describe the pretransitional behavior of relevant physical quantities in terms of power laws with critical exponents, which depend on the universality class of the phase transition [44–47].

The limiting behavior of the specific heat capacity at a second-order phase transition can be described with a power law of the form

$$c_p = A|\tau|^{-\alpha} + B, \quad (7)$$

with $\tau = (T - T_c)/T_c$. A is the critical amplitude, α is the critical exponent, T_c is the critical temperature (T and T_c in kelvin), and B is the background term. The different coefficients in Eq. (7) must be derived from (nonlinear) least-squares fitting of experimental data. The fact that ASC scans result directly in enthalpy $h(T)$ data [see Eq. (1)] allows for a substantial simplification. One can introduce the following quantity:

$$C = \frac{h - h_c}{T - T_c}, \quad (8)$$

which corresponds to the slope of the chord connecting $h(T)$ at T , with h_c at T_c . It can easily be shown that C has a power-law behavior of the form [33,35,36]

$$C = \frac{A}{1 - \alpha} |\tau|^{-\alpha} + B. \quad (9)$$

Both c_p and C have the same critical exponent, and either Eq. (7) or (9) can be used in fitting data to arrive at values for the critical exponent α and amplitude A . However, by considering the difference $(C - c_p)$, above or below T_c , the (unimportant) background term B drops out, resulting in

$$C - c_p = \frac{\alpha A}{1 - \alpha} |\tau|^{-\alpha}. \quad (10)$$

Taking the logarithm on both sides of Eq. (10) gives

$$\log_{10}(C - c_p) = \log_{10}\left(\frac{\alpha A}{1 - \alpha}\right) - \alpha \log_{10}|\tau|. \quad (11)$$

As a result, one obtains, sufficiently close to the critical point, a straight line with a negative slope, immediately giving the critical exponent α .

This procedure is strictly only applicable to second-order transitions, but for weakly first-order transitions it can be used for separate analysis of the data below and above the transition by allowing T_c and h_c in Eq. (8) to be adjustable parameters in fitting. The parameters T_c and h_c can be different for data below and above the transition. This is analogous to the upper stability limit of the nematic phase and the lower stability limit of the isotropic phase for the weakly first-order nematic-isotropic transition [35,37]. We have applied this approach to the present DIO phase transition data of c_p and h , excluding the data in the two-phase region.

A double logarithmic plot [see Eq. (11)] is shown in Fig. 6 for $(C - c_p)$ data of two different samples (A and B) as a function of the reduced temperature difference τ . It can be concluded that, within the experimental resolution, a negative slope of -0.88 ± 0.10 is consistent with the data. Thus, according to Eq. (11) this results in an effective critical exponent $\alpha = 0.88 \pm 0.10$. In Fig. 6, it can also be seen that $(C - c_p)$ above the transition $N_F - N_x$ is much larger than in the N_F phase below the transition. From Eq. (7) it immediately follows that the critical amplitude in the ferroelectric nematic phase, A_{N_F} , must be substantially smaller than the critical amplitude in the N_x phase. An estimate gives, for the ratio, $A_{N_F}/A_{N_x} = 0.39 \pm 0.03$.

B. Mixtures of DIO and RM734

1. Phase diagram

In order to clearly establish the temperatures of the $N_F - N_x$ and the $N_x - N$ transitions and the thermal behavior of the specific heat capacity $c_p(T)$ and of the specific enthalpy $h(T)$, eight different mixtures of DIO+RM734 were investigated by ASC. In Fig. 7, the temperature dependences of the specific heat capacity $c_p(T)$, from well in the ferroelectric nematic N_F phase to well into the paraelectric nematic N phase over the N_x phase, are compared for several DIO+RM734 mixtures. An overview of all the $N_F - N_x$ and $N_x - N$ transition temperatures is depicted in Fig. 8. The plotted points correspond with the maximum of the $c_p(T)$ data. These results indicate that a

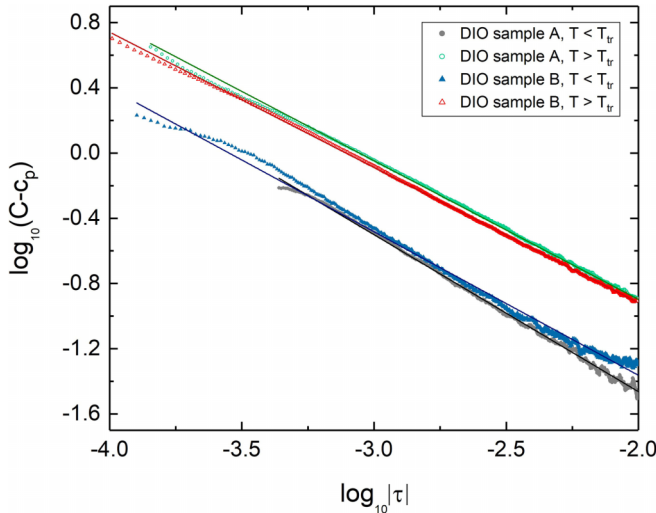


FIG. 6. Adiabatic scanning calorimetry results for the $N_F - N_x$ transition for two different samples of neat DIO. Double logarithmic plot for the difference $(C - c_p)$ expressed in $J/(g K)$ as a function of the reduced temperature difference τ [see Eq (8)]. The upper open green circles (sample A) and open red triangles (sample B) are for the data of $T > T_{tr}$. The gray solid circles (sample A) and blue solid triangles (sample B) are for the data of $T < T_{tr}$. The average slopes of the different trend lines are consistent with an effective critical exponent $\alpha \approx 0.88 \pm 0.10$.

narrowing of the N_x phase occurs by reducing the amount of DIO in the mixture. For the lowest DIO weight fraction $w_D = 0.118$ investigated, the data still indicate a narrow T range of $1.7^\circ C$ for a N_x phase. This suggests the disappearance of this phase at $w_D = 0$. This is in contradiction to the results in Ref. [31], where nonexistence of the N_x phase is reported for w_D values below ~ 0.40 . These latter data would mean a triple

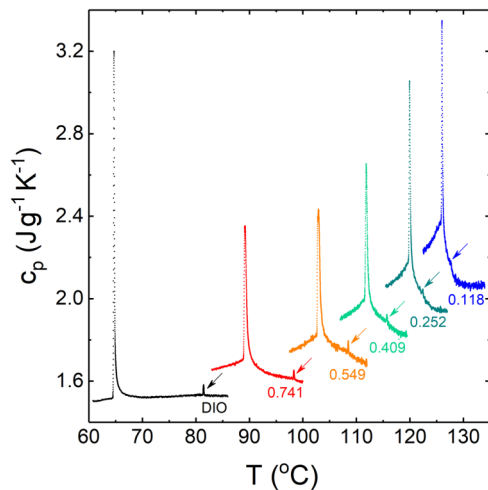


FIG. 7. Temperature dependence of the specific heat capacity c_p from well into the ferroelectric nematic phase N_F to well into the nematic phase N , crossing the $N_F - N_x$ and the $N_x - N$ transitions for DIO and five mixtures with weight fractions w_D of 0.741 (red), 0.549 (orange), 0.409 (green), 0.252 (dark green), and 0.118 (blue), respectively. The arrows point to the very weak signals of the $N_x - N$ transitions.

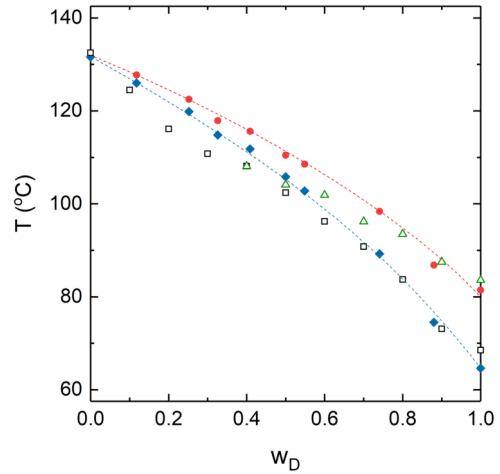


FIG. 8. Phase diagram for several mixtures of RM734+DIO. The red solid circles are present ASC values for the $N_x - N$ transition temperatures. The solid blue rhombs are the ASC results for the $N_F - N_x$ transition temperatures for DIO and the mixtures plus the data point at $w_D = 0$ for RM734 from Ref. [32]. The dashed red and blue curves represent quadratic trend lines through the data. The green open triangle and open black square symbols represent values derived from Fig. 2 in Ref. [31]. The triangles are, according to Ref. [31], for the $N_x - N$ transitions and the squares are for the $N_F - N_x$ transition for $w_D > 0.4$ and for the $N_F - N$ transition for $w_D < 0.4$.

point around $w_D = 0.40$, provided the two transition lines are first-order ones. Moreover, contrary to Ref. [31] our results reveal a clear curvature in w_D dependence of the transition temperatures for both transitions. This is clearly visible from the quadratic fits through the data points.

2. True latent heats at the transitions and width of the two-phase regions

Detailed analysis of $h(T)$ in combination with the corresponding $c_p(T)$ has revealed small two-phase regions for both transitions of all mixtures and discontinuous enthalpy changes, indicating an albeit very weakly first-order character of the transitions. Figure 9 gives an overview of the widths of the two-phase regions and Fig. 10 of the true latent heat values $L_{N_F - N_x}$ (J/g) and $L_{N_x - N}$ (J/g) for the $N_F - N_x$ transition (upper blue data points) and for the $N_x - N$ transition (lower red data points). The latent heats for the $N_x - N$ transitions are about a factor of 20 smaller than the ones for the $N_F - N_x$ transitions. The dotted lines in the figure are quadratic trend lines. The data point for the $N_x - N$ transition of neat RM734 is from Ref. [32].

As already shown in Fig. 5 for neat DIO, the enthalpy change associated with the transition between the N_x and the N phases is extremely small. The $c_p(T)$ data in Fig. 5 indicate the absence of pretransitional effects, making this transition purely, but very weakly, first order. The same characteristics were observed for the $N_x - N$ transitions in the eight investigated binary mixtures of RM734 and DIO. However, with decreasing DIO concentration this transition shifted to a temperature closer to that of the $N_F - N_x$ transition and also exhibited smaller peaks, becoming barely visible with

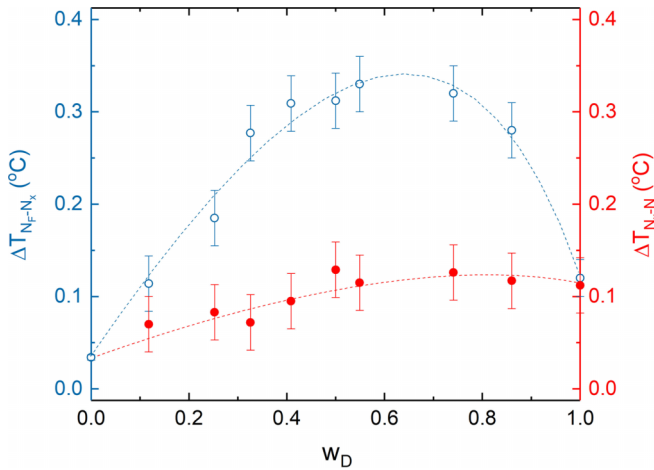


FIG. 9. Overview of the observed widths of the two-phase regions for neat DIO and RM734 and for the eight mixtures investigated. The upper blue (open circles) data points denote the $N_F - N_x$ transition. The blue data point at $w_D = 0$ is the value reported in Ref. [32] for the $N_F - N$ transition for RM734. The blue dashed line corresponds to a fit with a cubic equation. The lower red (solid circles) data points denote the $N_x - N$ transition and the red dashed line is from a quadratic fit. At $w_D = 0$ no red data point is plotted because no $N_x - N$ transition was reported in Ref. [32].

decreasing w_D on the pretransitional high-temperature $c_p(T)$ slope of the latter transition. Moreover, the corresponding widths and the latent heats gradually decreased with decreasing w_D . For the lowest $w_D = 0.118$, a latent heat value of only 0.002 ± 0.002 J/g was obtained.

The $N_F - N_x$ transition in the mixtures is also first order with decreasing latent heats upon decreasing w_D from the DIO

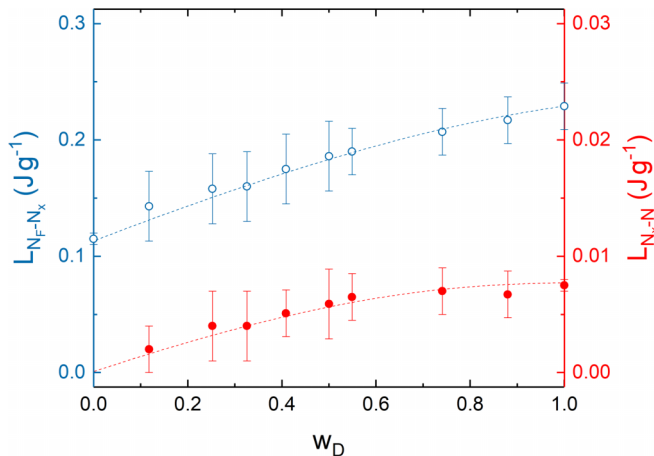


FIG. 10. True latent heat values $L_{N_F - N_x}$ and $L_{N_x - N}$ for the $N_F - N_x$ transition (upper open blue data points) and for the $N_x - N$ transition (lower solid red data points). Note that the right and left vertical axes use different scales. Thus the latent heats for the $N_x - N$ transitions are about a factor of 20 smaller than the ones for the $N_F - N_x$ transitions. The dashed lines are quadratic trend lines. The blue data point at $w_D = 0$ is the value reported in Ref. [32] for the $N_F - N$ transition of RM734. At $w_D = 0$ no red data point is plotted because no $N_x - N$ transition was reported in Ref. [32].

value of 0.23 ± 0.03 J/g to the value of 0.115 ± 0.005 J/g for RM734 [32]. As in the case of DIO and RM734, the mixtures also exhibit substantial, fluctuation-induced, pretransitional specific heat capacity changes near the $N_F - N_x$ transitions, in particular, in the high-temperature phases. In Fig. 7 it can be observed that the $c_p(T)$ variation extends well into the N phase above the $N_x - N$ transition. In fact, because of its smallness, the $c_p(T)$ peak associated with the $N_x - N$ transition has a negligible effect on the high-temperature $c_p(T)$ behavior associated with the $N_F - N_x$ transition.

3. Anomalous pretransitional specific heat capacity behavior at the $N_F - N_x$ transitions

As already pointed out for neat DIO in Sec. III A the fact that both $c_p(T)$ as well as $h(T)$ were obtained by ASC offers a specific and unique way of investigating pretransitional behavior by combining the specific heat capacity data $c_p(T)$ with the quantity C , derived from $h(T)$, and introduced in Eq. (8). As explained in Sec. III A, the method is in principle intended for second-order phase transitions, but can be extended to very weakly first-order phase transitions. This approach allows direct access to experimental values for the effective critical exponent α , introduced in the power-law expression of Eq. (4). This method was successfully used for RM734 [32] and for DIO above in Sec. III A (see also Fig. 6). Since the $N_F - N_x$ latent heats for the mixtures are as small as or smaller than for DIO (see Fig. 10), it can be expected that the method would be applicable for the mixtures. The increased two-phase width (see Fig. 10) of the mixtures is a concern, because two-phase region data have to be excluded from the analysis. In Fig. 11, an overview of log-log plots based on Eq. (11) and similar to Fig. 6 for DIO, is presented. As already pointed out in Sec. III A the slopes of these curves correspond with the effective critical exponent α values. It can be observed that with decreasing w_D the slope decreases from the DIO value (around 0.9) to the RM734 value (around 0.5 [32]). The curves on the low-temperature side of the transition exhibit (much) larger uncertainty because the critical amplitude [see Eq. (4)] for that phase is about 2.5 times smaller than those that were observed on the high-temperature side. Figure 12 gives an overview of the resulting values for the effective critical exponent α as a function of weight fraction w_D of DIO. Within the estimated uncertainties, an almost linear w_D dependence between the DIO and RM734 values can be observed.

IV. DISCUSSION

As already mentioned in the Introduction, more than a century ago Debye [5] and Born [6] discussed the possibility of a ferromagnetic phase by extending the ferromagnetic Weiss model to molecular electric dipoles, but only recently such phase behavior was observed experimentally. In 2017 two different molecules were reported to exhibit ferroelectriclike features independently by two different groups. One molecule was RM734 [7–12] and the other was DIO [8]. In the meantime, many more compounds from both the RM734 family [15] and the DIO family [20] have been reported to exhibit nematic ferroelectricity. The fact that RM734 and DIO are members of separate molecular families with quite different

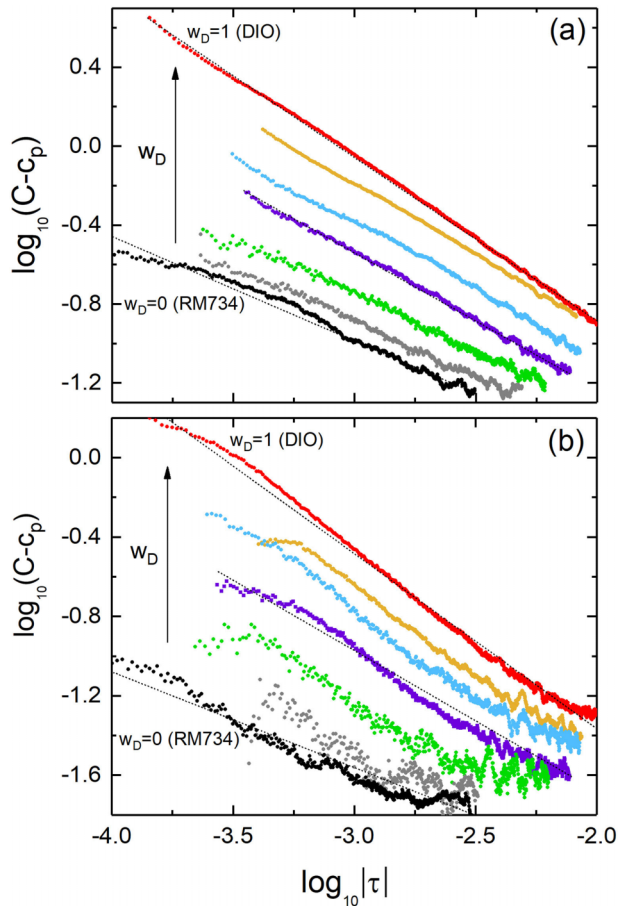


FIG. 11. Double logarithmic plot for the difference $(C-c_p)$, expressed in $J/(g\ K)$ as a function of the reduced temperature difference τ [see Eq. (8)]. The upper panel (a) shows data above the transition temperature T_{tr} . The lower panel (b) shows data below T_{tr} . Red data points are for neat DIO and the black ones for neat RM734. The intermediate curves are for mixtures of DIO and RM734 with weight fraction $w_D = 0.741$ (orange), $w_D = 0.549$ (blue), $w_D = 0.409$ (violet), $w_D = 0.252$ (green), and $w_D = 0.118$ (gray). Some of the data sets have been shifted upward for display reasons. The slopes of the curves correspond to the effective critical exponent α of Eq. (8).

molecular structures makes ferronematic behavior a surprise at first sight. This has motivated investigations of differences and similarities in phase behavior of these molecules and of their mixtures [29,31].

In the past, high-resolution calorimetric studies have played a significant role in providing information on energy effects near many liquid crystal phase transitions [44,45,48,49]. In fact, the many different phases and phase transitions make liquid crystals excellent model systems for testing general phase transition and critical phenomena concepts. The first-order or second-order (or continuous) nature of transitions and their critical exponents and universality class have been investigated extensively. Adiabatic scanning calorimetry has proven to be an important tool to discriminate between first-order and second-order transitions and render high-resolution information on pretransitional heat capacity behavior.

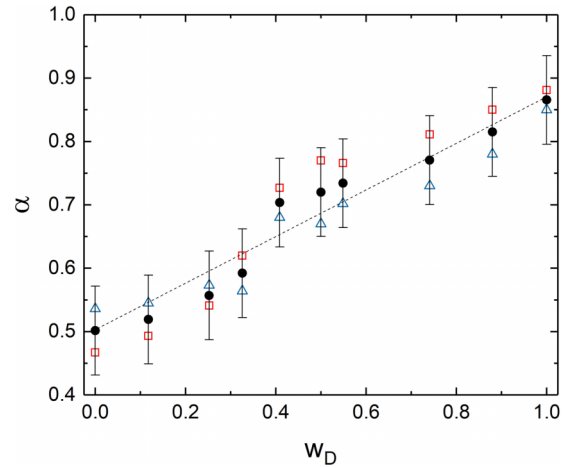


FIG. 12. Comparisons, as a function of the weight fraction of DIO, between the effective critical exponent α values [see Eq. (4)] at the $N_F - N_x$ transition for neat RM734 (to the left) and neat DIO (to the right) and for eight different mixtures of these compounds. The open (red) squares are from $c_p(T)$ data above the transitions and the open (blue) triangles below the transition. The solid (black) circles are average values and the dashed line shows a linear fit through these data.

A previous paper [32] presented the results of a detailed ASC investigation of the ferroelectric nematic to nematic transition ($N_F - N$) transition of RM734. As already pointed out in the Introduction the transition was proven to be very weakly first order with a true latent heat $L = 0.115 \pm 0.005$ J/g. The pretransitional specific heat capacity behavior in the high-temperature nematic phase was found to be substantially larger than in the low-temperature ferronematic phase. For most phase transitions the opposite is common. Analysis of this pretransitional behavior resulted in a critical exponent [see Eq. (7)] $\alpha = 0.50 \pm 0.05$. This value of the critical exponent suggested (although first order) the transition to be close to a tricritical point.

From our results on DIO, presented in Sec. III A, some similarities and differences with RM734 can be observed. As already established, an important difference with RM734 is the presence of the N_x phase between the N_F and the N phases and the presence of an additional $N_x - N$ phase transition. This transition is weakly first order, with a latent heat $L = 0.0075 \pm 0.0005$ J/g and exhibits no pretransitional effects (see Fig. 5). The temperature dependence of $c_p(T)$ and $h(T)$ around the $N_F - N_x$ transition (see Figs. 3 and 4) is similar to that of the $N_F - N$ transition of RM734. The $N_F - N_x$ transition of DIO is also weakly first order, albeit with a larger latent heat $L = 0.23 \pm 0.03$ J/g which is about twice that of RM734. Power-law analysis (see Sec. III A and Fig. 6) of the pretransitional specific heat capacity resulted in an effective critical exponent $\alpha = 0.88 \pm 0.10$. This is an unusual value which is quite different from the $\alpha = 0.50 \pm 0.05$ observed for RM734. This, likely being a crossover value, cannot obviously be linked to a specific type of universality class.

In a further effort to find insight into the similarities and differences in the phase transition behavior of DIO and RM734, we carried out ASC runs for eight mixtures of these

compounds. From these measurements and in the phase diagram in Fig. 8 we did not find any evidence of phase separation, thus confirming the complete miscibility reported by Chen *et al.* [31]. However, from the comparison in Fig. 8 between our phase transition temperatures and the ones from Ref. [31], two significant differences are observed. First, in our case the N_x phase persists over the entire concentration range (at least from $w_D = 0.12$ to 1.0) and does not disappear for weight fractions below $w_D \approx 0.40$ as was reported in [31]. Second, our data show curvature (see the quadratic fits in Fig. 8), deviating from the linearity that was presumed in Ref. [31]. This discrepancy, and the quoted linearity, are most likely the result of the lower resolution of the transition temperature determination in Ref. [31]. Chen *et al.* [31] tested ideal mixing of the paraelectric and ferroelectric phases on the basis of an expression derived by Van Hecke [50] on the basis of the so-called equal G analysis. In this approach, the total Gibbs energies between two phases in equilibrium are set equal to describe phase coexistence. Ideal as well as nonideal systems under constant pressure have been considered. For a two-component ideal mixture (absence of excess Gibbs energies) and provided that the heat capacity effects are small compared to transition entropies, the following expression was obtained [50] for the transition temperatures as a function of the mole fraction x of component 2:

$$T(x) = \frac{(1-x)\Delta S_1 T_1 + x\Delta S_2 T_2}{(1-x)\Delta S_1 + x\Delta S_2}. \quad (12)$$

T_1 and T_2 are the transition temperatures of the pure components and ΔS_1 and ΔS_2 are the corresponding (constant) transition entropies. Provided the values of T_1 and T_2 of the pure compounds are known, the number of unknown parameters on the right-hand side of this equation can be reduced to 1, allowing for a single parameter fit to experimental data of the transition temperatures of the mixtures:

$$T(x) = \frac{(1-x)T_1 + xsT_2}{(1-x) + xs}, \quad (13)$$

with $s = \Delta S_2/\Delta S_1$ the fitting parameter. From Eq. (13) it can immediately be observed that $T(x)$ (with x the mole fraction of component 2) is only linear for $s = 1$. For values of $s > 1$ the curve $T(x)$ is convex shaped and for $s < 1$ it is concave shaped. However, this does not indicate that the system is nonideal [50].

In order to test whether Eq. (13) is applicable to our $N_F - N_x$ phase transition data, we have converted the data from a $T(w_D)$ representation, with w_D the weight fraction of DIO, as in Fig. 8, to $T(x)$, with x the mole fraction of DIO, i.e., compound number 2, in Eq. (13) using the molecular weights $MW_{RM734} = 423$ g/mol and $MW_{DIO} = 510$ g/mol. Figure 13 gives the $N_F - N_x$ and the $N_x - N$ transition temperature data versus the mole fraction of DIO. Before using Eq. (13) in the data analysis, we can consider some boundary conditions for ideal systems on the slopes of the coexistence curve at $x = 0$ and $x = 1$. The following two slope equations apply [50]:

$$D_0 \equiv \left. \frac{\partial T}{\partial x} \right|_{x \rightarrow 0} = -s(T_1 - T_2), \quad (14)$$

$$D_1 \equiv \left. \frac{\partial T}{\partial x} \right|_{x \rightarrow 1} = (T_2 - T_1)/s. \quad (15)$$

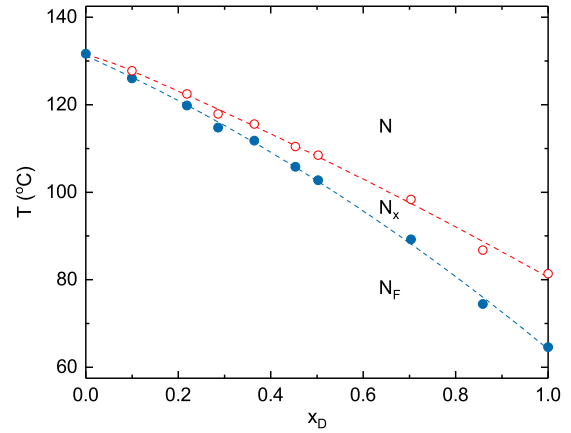


FIG. 13. Transition temperatures as a function of the mole fraction of DIO. The red open circles are data of the $N_x - N$ transition temperatures, and the solid blue circles are the results for the $N_F - N_x$ transition temperatures of DIO and of the mixtures and for the $N_F - N$ transition temperature of RM734 (at $x = 0$), reported in Ref. [32]. The dashed red and blue curves represent quadratic trend lines through the corresponding data points.

Making the product of Eqs. (14) and (15) results in

$$D_{0,1} \equiv \left. \frac{\partial T}{\partial x} \right|_0 \left. \frac{\partial T}{\partial x} \right|_1 = (T_2 - T_1)^2. \quad (16)$$

In order to arrive at initial slope values at $x = 0$ and $x = 1$ for the $N_F - N_x$ transitions we have used the following very good fitting result: $T(x) = -19.83x^2 - 47.2x + 404$ (see Fig. 13). This gives us the derivative result $D_0 = -47.2 \pm 0.2$ K and $D_1 = -87 \pm 1$ K. The product $D_{0,1} = D_0 D_1 = 4098 \pm 65$ K² compares reasonably well with $(T_2 - T_1)^2 = (67 \pm 1)^2 = 4489 \pm 135$ K². Equations (14) and (15) also allowed us to arrive at values of $s = \Delta S_2/\Delta S_1$. From D_0 we obtain $s = 0.71 \pm 0.02$ and from D_1 we get $s = 0.77 \pm 0.02$. Fitting the transition temperatures with s as an adjustable parameter in Eq. (13) results in $s = 0.78 \pm 0.03$.

The above values can be compared with the experimental ratio $s = \Delta S_{DIO}/\Delta S_{RM734}$ which can either be calculated from the true latent heat values L or from Δh_{tr} which have been reported in Sec. III A. Using only the true latent heat values resulting in $s = 2.00$, which differs by a large amount from the above values. However, using the (total) Δh_{tr} values of Sec. III A yields $s = \Delta S_{DIO}/\Delta S_{RM734} = 0.73/1.07 = 0.68 \pm 0.12$, which is close to the slope results discussed above. This indicates that it is necessary to include in ΔS the pretransition fluctuation contribution to be consistent with the results obtained by the analysis using Eqs. (12)–(16). The comparability of the s value seems to confirm the proposed ideality [31] of the binary DIO+RM734 system, albeit with a nonlinear $T(x)$ curve.

The procedure established in Sec. III A to arrive at Δh_{tr} for the neat DIO and RM734 can be applied to the mixtures as well. The results of this analysis are summarized in Fig. 14. An almost linear weight fraction w_D dependence can be observed, which is decreasing with w_D , which is opposite to what can be seen in Fig. 9 for the latent heat.

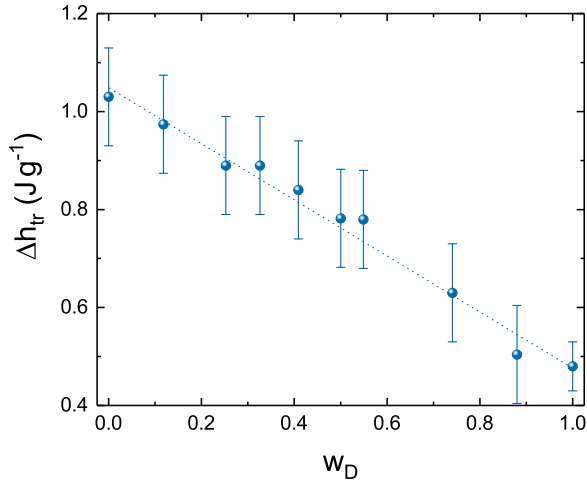


FIG. 14. Total specific enthalpy change Δh_{tr} associated with the transitions from the N_F - N_x transitions as a function of the weight fraction w_D of DIO [see Eq. (3)]. The point at $w_D = 0$ is for the N_F - N transition of RM734 [32].

Equations (13)–(16) have also been applied to the transition temperature data for the N_x - N transition. For the slope analysis at $x = 0$ and $x = 1$ we used the fit equation $T(x) = -8.46x^2 - 42.9x - 405$ (see Fig. 13). The derivatives resulted in $D_0 = -42.9 \pm 0.3$ and $D_1 = -60 \pm 1$. From $T_2 - T_1 = 50 \pm 1$ K and D_0 we obtain $s = 0.86 \pm 0.03$ and from D_1 we get $s = 0.83$. The product $D_{0,1} = D_0 D_1 = 2567 \pm 70$ K² compares well with $(T_2 - T_1)^2 = (50.0)^2 = 2500 \pm 100$ K². Fitting the transition temperatures with s as an adjustable parameter in Eq. (13) results in $s = 0.88$. In this case comparison with the experimental ratio $s = \Delta S_{DIO} / \Delta S_{RM734}$ was not feasible, because no N_x - N transition has been detected [32] in compound 1 (RM734).

Detailed analysis (see Sec. III B) of the specific enthalpy $h(T)$ data in combination with the specific heat capacity $c_p(T)$ data confirmed the first-order character of both the N_F - N_x and the N_x - N transitions in all the investigated mixtures. While the two-phase region for N_x - N gradually decreased with decreasing weight fraction of DIO, substantially wider two-phase regions were observed in the range of w_D around 0.5 for the N_F - N_x transitions (see Fig. 9). However, for both types of transition the true latent heats L gradually decreased with decreasing w_D (see Fig. 10). Power-law analysis for the mixtures, similar to the ones performed for neat RM734 and DIO, resulted in a set of effective critical exponent α values intermediate between those of RM734 ($\alpha = 0.50 \pm 0.05$) and of DIO ($\alpha = 0.88 \pm 0.10$), with an almost linear dependence on w_D (see Fig. 12). As the RM734 value could be associated with the possibility of a nearby tricritical point [32], the DIO

value and the evolution with w_D cannot obviously be linked to any specific universality class or a crossover between two different (known) universality classes [51].

V. SUMMARY AND CONCLUSIONS

High-resolution adiabatic scanning calorimetry (ASC) has been used to obtain simultaneously the temperature dependence of the specific enthalpy $h(T)$ on the specific heat capacity $c_p(T)$ of the compound 2,3',4',5'-tetrafluoro[1,1'-biphenyl]-4-yl-2,6-difluoro-4-(5-propyl-1,3-dioxan-2-yl)benzoate (DIO) and on several of its mixtures with 4-[(4-nitrophenoxy)carbonyl]phenyl 2,4-dimethoxybenzoate (RM734). Both compounds exhibit a low-temperature ferroelectric nematic phase (N_F) and a high-temperature nematic phase (N). However, in DIO these two phases are separated by an intermediate phase (N_x). From the detailed data of $h(T)$ and $c_p(T)$, we found that the intermediate N_x phase was present in all the mixtures over the complete composition range, albeit with strongly decreasing temperature width for that phase with decreasing mole fraction of DIO (x_{DIO}). The x_{DIO} dependence of the transition temperatures for both the transitions could be well described by a quadratic function. Both these transitions were weakly first order. The true latent heat of the N_x - N transition of DIO was as low as $L = 0.0075 \pm 0.0005$ J/g and was $L = 0.23 \pm 0.03$ J/g for the N_F - N_x transition, which is about twice the previously reported value of 0.115 J/g for the N_F - N transition in RM734. In the mixtures both transition latent heats decrease gradually with decreasing x_{DIO} . At all the N_x - N transitions pretransition fluctuation effects are absent and these transitions are purely, though very weakly, first order. As observed in RM734 the transition from the N_F to the higher-temperature phase exhibits substantial pretransitional behavior, in particular, in the high-temperature phase. Power-law analysis of $c_p(T)$ resulted in an effective critical exponent $\alpha = 0.88 \pm 0.1$ for DIO. In the mixtures the effective α value decreased with decreasing x_{DIO} to $\alpha = 0.50 \pm 0.05$, the value reported for RM734 [32]. Ideal mixture analysis [50] of the phase diagram was consistent with ideal mixture behavior, provided the total transition enthalpy change was used in the analysis.

ACKNOWLEDGMENTS

G.C. acknowledges financial support from Project No. P1-0125 of the Slovene Research Agency. W.J. acknowledges the China Scholarship Council (CSC) for a Ph.D. scholarship. G.H.M. acknowledges project funding by Diamond Light Source (station B23).

- [1] P. G. de Gennes and J. Prost, *The Physics of Liquid Crystals* (Oxford University Press, New York, 1993).
 [2] L. J. Yu and A. Saupe, Observation of a Biaxial Nematic Phase in Potassium Laurate-1-Decanol-Water, *Phys. Rev. Lett.* **45**, 1000 (1980).

- [3] S. Chandrasekhar, B. R. Ratna, B. K. Sadashiva, and V. N. Raja, Thermotropic biaxial nematic liquid-crystal, *Mol. Cryst. Liq. Cryst.* **165**, 123 (1988).
 [4] G. Nounesis, S. Kumar, S. Pfeiffer, R. Shashidhar, and C. W. Garland, Experimental Observation of a Transition between

- Two Uniaxial Nematic Liquid-Crystal Phases, *Phys. Rev. Lett.* **73**, 565 (1994).
- [5] P. Debye, Some results on a kinetic theory of insulators, *Phys. Z.* **13**, 97 (1912).
- [6] M. Born, About anisotropic liquids. Attempt of a theory of liquid crystals and the electric Kerr effect in liquids, *Sitzungsber. Preuss. Akad. Wiss.* **30**, 614 (1916).
- [7] R. J. Mandle, S. J. Cowling, and J. W. Goodby, A nematic to nematic transformation exhibited by a rod-like liquid crystal, *Phys. Chem. Chem. Phys.* **19**, 11429 (2017).
- [8] H. Nishikawa, K. Shirishita, H. Higuchi, Y. Okumura, Y. Haseba, S. I. Yamamoto, K. Sago, and H. Kukuchi, A fluid liquid-crystal material with highly polar order, *Adv. Mater.* **29**, 1702354 (2017).
- [9] R. J. Mandle, S. J. Cowling, and J. W. Goodby, Rational design of rod-like liquid crystals exhibiting two nematic phases, *Chem Eur. J.* **23**, 14554 (2017).
- [10] A. Mertelj, L. Cmok, N. Sebastián, R. J. Mandle, R. R. Parker, A. C. Whitwood, J. W. Goodby, and M. Čopič, Splay Nematic Phase, *Phys. Rev. X* **8**, 041025 (2018).
- [11] R. J. Mandle and A. Mertelj, Orientational order in the splay nematic ground state, *Phys. Chem. Chem. Phys.* **21**, 18769 (2019).
- [12] N. Sebastián, L. Cmok, R. J. Mandle, M. Rosario de la Fuente, I. Drevenšek Olenik, M. Čopič, and A. Mertelj, Ferroelectric-Ferroelastic Phase Transition in a Nematic Liquid Crystal, *Phys. Rev. Lett.* **124**, 037801 (2020).
- [13] R. L. M. Connor and R. J. Mandle, Chemically induced splay nematic phase with micron scale periodicity, *Soft Matter* **16**, 324 (2020).
- [14] X. Chen, E. Korblova, D. Dong, X. Wei, R. Shao, L. Radzihovsky, M. A. Glaser, J. E. MacLennan, D. Bedrov, D. M. Walba, and N. Clark, First-principles experimental demonstration of ferroelectricity in a thermotropic nematic liquid crystal: Polar domains and striking electro-optics, *Proc. Natl. Acad. Sci. USA* **117**, 14021 (2020).
- [15] R. J. Mandle, S. J. Cowling, and J. W. Goodby, Structural variants of RM734 in the design of splay nematic materials, *Liq. Cryst.* **48**, 1780 (2021).
- [16] X. Chen, E. Korblova, M. A. Glaser, J. E. MacLennan, D. M. Walba, and N. Clark, Polar in-plane surface orientation of a ferroelectric nematic liquid crystal: Polar monodomains and twisted state electro-optics, *Proc. Natl. Acad. Sci. USA* **118**, e2104092118 (2021).
- [17] S. Brown, E. Cruickshank, J. M. D. Storey, C. T. Imrie, D. Pocięcha, M. Majewska, A. Makal, and E. Gorecka, Multiple polar and non-polar nematic phases, *Phys. Chem. Chem. Phys.* **22**, 2506 (2021).
- [18] F. Caimi, G. Nava, R. Barboza, N. A. Clark, E. Korblova, D. Walba, T. Bellini, and L. Lucchetti, Surface alignment of ferroelectric nematic liquid crystals, *Soft Matter* **17**, 8130 (2021).
- [19] A. Manabe, M. Bremer, and M. Kaska, Ferroelectric nematic phase at and below room temperature, *Liq. Cryst.* **48**, 1079 (2021).
- [20] J. Li, H. Nishikawa, J. Kougo, J. Zhou, S. Dai, W. Tang, X. Zhao, Y. Hisai, M. Huang, and S. Aya, Development of ferroelectric nematic fluids with giant- ϵ dielectricity and nonlinear optical properties, *Sci. Adv.* **7**, eabf5047 (2021).
- [21] R. Saha, P. Nepal, C. Feng, M. S. Hossein, J. T. Gleeson, S. Sprunt, R. J. Twieg, and A. Jáklı, Multiple ferroelectric nematic phases of highly polar liquid crystal compounds, [arXiv:2104.06520](https://arxiv.org/abs/2104.06520).
- [22] R. Saha, P. Nepal, C. R. Feng, M. S. Hossain, M. Fukuto, R. P. Li, J. T. Gleeson, S. Sprunt, R. J. Twieg, and A. Jáklı, Multiple ferroelectric nematic phases of a highly polar liquid crystal compound, *Liq. Cryst.* **49**, 1784 (2022).
- [23] P. Rudquist, Revealing the polar nature of a ferroelectric nematic by means of circular alignment, *Sci. Rep.* **11**, 24411 (2021).
- [24] R. Barboza, S. Marni, F. Ciciulla, F. A. Mir, G. Nava, F. Caimi, A. Zaltron, N. A. Clark, T. Bellini, and L. Lucchetti, Explosive electrostatic instability of ferroelectric liquid droplets on ferroelectric surfaces, *Proc. Natl. Acad. Sci. USA* **119**, e2207858119 (2022).
- [25] H. Nishikawa, K. Sano, and F. Araoka, Anisotropic fluid with phototunable dielectric permittivity, *Nat. Commun.* **13**, 1142 (2022).
- [26] H. Nishikawa, K. Sano, S. Kurihara, G. Watanabe, A. Nihonyanagi, B. Dhara, and F. Araoka, Nano-clustering mediates phase transitions in a diastereomerically-stabilized ferroelectric nematic system, *Commun. Mater.* **3**, 89 (2022).
- [27] B. Basnet, M. Rajabi, H. Wang, P. Kumari, K. Thapa, S. Paul, M. O. Lavrentovich, and O. O. Lavrentovich, Soliton walls paired by polar surface interactions in a ferroelectric nematic liquid crystal, *Nat. Commun.* **13**, 3932 (2022).
- [28] M. T. Máthé, Á. Buka, A. Jáklı, and P. Salamon, Ferroelectric nematic liquid crystal thermomotor, *Phys. Rev. E* **105**, L052701 (2022).
- [29] X. Chen, E. Korblova, G. Freychet, M. Zhernenkov, V. M. J. Magrini, J. E. MacLennan, D. M. Walba, and N. A. Clark, Antiferroelectric smectic ordering as a prelude to a ferroelectric nematic: Introducing the smectic Z_A phase, [arXiv:2112.14222](https://arxiv.org/abs/2112.14222).
- [30] N. Sebastián, M. Čopič, and A. Mertelj, Ferroelectric nematic phases, *Phys. Rev. E* **106**, 021001 (2022).
- [31] X. Chen, Z. Zhu, M. J. Magrini, E. Korblova, C. S. Park, M. A. Glaser, J. E. MacLennan, D. M. Walba, and N. A. Clark, Ideal mixing of paraelectric and ferroelectric nematic phases in liquid crystals of distinct molecular species, *Liq. Cryst.* **49**, 1531 (2022).
- [32] J. Thoen, E. Korblova, D. M. Walba, N. Clark, and C. Glorieux, Precision adiabatic scanning calorimetry of a nematic-ferroelectric nematic phase transition, *Liq. Cryst.* **49**, 780 (2022).
- [33] J. Thoen, H. Marynissen, and W. Van Dael, Temperature dependence of the enthalpy and the heat capacity of the liquid crystal octylcyanobiphenyl (8CB), *Phys. Rev. A* **26**, 2886 (1982).
- [34] J. Thoen, E. Bloemen, H. Marynissen, and W. Van Dael, High-resolution calorimetric investigation of phase transitions in liquids, in *Proceedings of the 8th Symposium on Thermal Properties*, edited by J. V. Sengers (American Society of Mechanical Engineers, New York, 1982), pp. 422–427.
- [35] J. Thoen, Thermal investigations of phase transitions in thermotropic liquid crystals, *Int. J. Mod. Phys. B* **9**, 2157 (1995).
- [36] J. Thoen, G. Cordoyiannis, and C. Glorieux, Investigation of phase transitions in liquid crystals by means of adiabatic scanning calorimetry, *Liq. Cryst.* **36**, 669 (2009).
- [37] J. Thoen, High resolution adiabatic scanning calorimetry and heat capacities, in *Heat Capacities: Liquids, Solutions and*

- Vapours*, edited by E. Wilhelm and T. Letcher (RSC Publishing, Cambridge, UK, 2010), pp. 287–328.
- [38] J. Thoen, J. Leys, and C. Glorieux, Adiabatic scanning calorimeter, European Patent EP 2 91328 B1 (02 September 2015), U.S. Patent No. 9,310,263 B2 (12 April 2016).
- [39] J. Leys, P. Losada-Pérez, C. Glorieux, and J. Thoen, Application of a novel type of adiabatic scanning calorimeter for high-resolution thermal data near the melting point of gallium, *J. Therm. Anal. Calorim.* **117**, 173 (2014).
- [40] J. Thoen, Enthalpy measurements of condensed matter by Peltier-element-based adiabatic scanning calorimetry (pASC), in *Enthalpy and Internal Energy: Liquids, Solutions and Vapours*, edited by E. Wilhelm and T. Letcher (RSC Publishing, Croydon, UK, 2018), pp. 77–95.
- [41] J. Thoen, G. Cordoyiannis, P. Losad-Pérez, and C. Glorieux, High-resolution investigation by Peltier-element-based adiabatic scanning calorimetry of binary liquid crystal mixtures with enhanced nematic ranges, *J. Mol. Liq.* **340**, 117204 (2021).
- [42] J. Thoen, G. Cordoyiannis, and C. Glorieux, Adiabatic scanning calorimetry investigation of the melting and order-disorder phase transitions in the linear alkanes heptadecane and nonadecane and some of their binary mixtures, *J. Chem. Thermodyn.* **163**, 106596 (2021).
- [43] J. Leys, P. Losada-Pérez, E. Slenders, C. Glorieux, and J. Thoen, Investigation of the melting behavior of the reference materials biphenyl and phenyl salicylate by a new type adiabatic scanning calorimeter, *Thermochim. Acta* **582**, 68. (2014).
- [44] G. B. Kasting, C. W. Garland, and K. J. Lushington, Critical heat capacity of octylcyanobiphenyl (8CB) near the nematic-smectic *A* transition, *J. Phys.* **41**, 879 (1980).
- [45] G. B. Kasting, K. J. Lushington, and C. W. Garland, Critical heat capacity near nematic-smectic *A* transition in octyloxy cyanobiphenyl in the range 1–2000 bar, *Phys. Rev. B* **22**, 321 (1980).
- [46] H. E. Stanley, *Introduction to Phase Transitions and Critical Phenomena* (Oxford University Press, New York, 1971).
- [47] M. A. Anisimov, *Critical Phenomena in Liquids and Liquid Crystals* (Gordon and Breach, Philadelphia, 1991).
- [48] J. Thoen, Thermal investigations of phase transitions in thermotropic liquid crystals, in *Liquid Crystals in the Nineties and Beyond*, edited by S. Kumar (World Scientific, Singapore, 1995), pp. 19–80.
- [49] C. W. Garland, Calorimetric studies, in *Liquid Crystals, Experimental Study of Physical Properties and Phase Transitions*, edited by S. Kumar (Cambridge University Press, Cambridge, 2001), pp. 240–294.
- [50] G. R. Van Hecke, The equal *G* analysis. A comprehensive thermodynamic treatment for the calculation of liquid crystalline phase diagrams, *J. Phys. Chem.* **89**, 2058 (1985).
- [51] A. Pelissetto and E. Vikari, Critical phenomena and renormalization-group theory, *Phys. Rep.* **368**, 549 (2002).